Geophys. J. Int. (1992) **110,** 501–517

Rupture geometry from high-precision relative hypocentre locations of microearthquake clusters

Nicholas Deichmann and Mariano Garcia-Fernandez*
Swiss Seismological Service, Institute of Geophysics, ETH-Hönggerberg, CH-8093 Zürich, Switzerland

Accepted 1992 March 20. Received 1992 March 19; in original form 1991 October 21

SUMMARY

In 1987, two microearthquake sequences, with a duration of about a week each and consisting of 37 and 46 events respectively, occurred in the upper crust below the Jura Mountains of northern Switzerland. The seismograms within each sequence exhibit a high degree of similarity, indicating tight clustering of hypocentres and similar focal mechanisms. Using a cross-correlation technique applied to the seismograms in the time domain, together with a new least-squares adjustment procedure, it was possible to determine relative hypocentre locations of the earthquakes in each cluster with a precision of a few tens of metres. The results show that hypocentres of events with the same focal mechanism lie on a plane which coincides exactly with one of the nodal planes of the fault-plane solution, and that consequently swarm-like sequences of similar earthquakes are due to repeated slip on the same fault. In one case, slip occurred as right-lateral motion on a steeply dipping plane striking in WNW–ESE direction, whereas the other case corresponds to left-lateral slip on two almost vertical planes striking roughly N–S. In 1988, an additional earthquake triplet occurred on a WNW–ESE oriented normal fault nearby. All three mechanisms are consistent with a general NNW–SSE oriented direction of maximum crustal shortening and a corresponding WSW–ENE oriented extension. Repeated slip on the same fault is indicative of a large degree of heterogeneity and of short-term temporal variability of both frictional resistance and stress distribution on the fault. An explanation for the occurrence of such swarm-like seismic activity in terms of barriers or asperities would require that shear stress on the unbroken patches increase from one event to the next. Since, however, the overall shear stress would be expected to decrease as a consequence of the stress released in each event, a more plausible mechanism involves pore-pressure fluctuations, caused by fluids under suprahydrostatic pressures migrating upward through pre-existing zones of weakness in the crust.

Key words: cross-correlation, earthquake swarms, fault plane, master event location, pore pressure.

INTRODUCTION

In recent years, small earthquakes in numerous parts of the world have been observed to occur in clusters of events with almost identical signal character. Most often, individual events occur within seconds to hours of each other and the whole sequences are spread out over weeks, in a swarm-like fashion. In some cases, such similar events have also been observed with in between quiescent times of a year or more. Based on the striking signal similarity of four magnitude 2.7 earthquakes in central California, Geller & Mueller (1980) concluded that such events must occur within about one quarter of a wavelength from each other (a few hundred metres, in their case) and that they represent repeated rupturing of the same asperity. Tsujiura (1983a, b) analysed in great detail numerous clusters of similar earthquakes in Japan and, following Hamaguchi & Hasegawa (1975), called them earthquake families. He conjectured that such families are characteristic of earthquake swarms and are due to repeated slip on the same fault plane, whereas foreshock–mainshock sequences, featuring more diverse signal forms, represent independent faulting in a complex and heterogeneous fault zone.

* Now at: Estacion Volcanologica de Canarias, E-38080 La Laguna, Tenerife, Spain.

In order to investigate the spatial distribution of the individual events in a cluster, several authors have applied cross-correlation techniques either in the frequency or in the time domain to such similar signals. Using a technique, that was first applied by Nakamura (1978) to the analysis of moonquakes and that is based on the phase of the cross-spectrum of two events, Poupinet, Ellsworth & Fréchet (1984) and Fréchet (1985) showed that the point sources of doublets of similar microearthquakes along the San Andreas Fault were often separated by less than 10 m. The same technique was also applied by Ito (1985, 1990) to several earthquake swarms in Japan, by Scherbaum & Wendler (1986) to earthquakes beneath the Swabian Jura, SW Germany, and by Fremont & Malone (1987) to several clusters below Mount St. Helens. Time-domain cross-correlations were applied to a cluster in southern Sweden (Slunga, Norman & Glans 1984), to the Remiremont sequence of 1984/85 in the Vosges Mountains, France (Plantet & Cansi 1988), to a six-event cluster at 23 km depth below the Molasse Basin near Winterthur, Switzerland (Deichmann 1987), to three groups of earthquakes along the North Anatolian Fault (Logan 1987), to clusters in central Italy (Console & Di Giovambattista 1987) and to two earthquake sequences in Utah (Pechmann & Thorbjarnardottir 1990). All these investigations show that families of similar earthquakes cluster tightly in space and suggest that the similarity of waveforms is due to a common focal mechanism.

In this paper we want to present an investigation of the temporal and spatial distribution of events constituting two clusters and a triplet of microearthquakes that occurred in northern Switzerland. The cross-correlation was performed in the time domain, and a new least-squares adjustment procedure was used to improve the precision of the relative arrival times and to estimate their uncertainty. The results allow us to demonstrate that similar earthquakes correspond to repeated slip on the same fault plane and to investigate the relation between cluster geometry, focal mechanism and orientation of the regional stress field. In addition, we address the problem of how repeated slip on the same fault is possible within short time periods.

TECTONIC SETTING

The two larger earthquake clusters analysed in this study occurred in January and April of 1987 in the central part of northern Switzerland. The earthquakes are situated in a seismically active region that extends southward from the Rhinegraben and Black Forest of Germany into the Swiss Jura Mountains. The epicentre of the first cluster was located near the town of Günsberg while the second one occurred 30 km further to the northeast, near the town of Läufelfingen. Focal depths of 6 to 7 km place the hypocentres in the crystalline basement below the southern and northern margin of the Folded Jura Mountains (Figs 1 and 13). The maximum magnitude of the earthquakes was 2.6 in the Günsberg cluster and 3.4 in the Läufelfingen cluster. In 1988 April, an additional earthquake triplet with magnitudes between 1.5 and 1.9 occurred near the town of Zeglingen, 2 km NE of Läufelfingen, at a depth of about 9 km. This additional cluster will be discussed separately at the end of the paper. The hypocentral parameters of all three clusters are listed in Table 1.

INSTRUMENTATION

During 1987 and 1988, four different seismograph arrays were operative in northern Switzerland and southern Germany: the Swiss national telemetry network with centralized digital data acquisition at the Institute of Geophysics of the ETH in Zürich, a local eight-station telemetry network recording on digital cassettes, a small temporary array of eight single stations in the area east of Basel recording continuously on analogue magnetic tape, and several digital seismographs in the southern Black Forest and around Basel operated by the University of Karlsruhe (Germany).

Whereas all the available data were used for the absolute location of the clusters and for the construction of fault-plane solutions, only data from one of the stations of the national network (BAL) and from the eight-station digital array were used for the determination of relative locations. This latter array consists of six vertical component seismometers (RBF, TSB, GEF, ENB, GIF, EIT) and two three-component seismometers (CHE, ACB) (see Fig. 1). The signals are recorded at station CHE by a digital event recorder, with a sampling rate of 100 Hz. Because of the FM-telemetry, the dynamic range of the remote stations is limited to about 60 db. Only the locally recorded station (CHE) can full exploit the more than 100 db of the gain-ranging amplifier in the recording instrument.

ABSOLUTE LOCATIONS

The absolute locations of the two earthquake clusters were determined with the widely used computer program HYPO71 (Lee & Lahr 1972). The velocity model consists of a 1 km thick near-surface layer with 4.5 km s^{-1}, an upper crustal crystalline velocity of 6.0 km s^{-1} down to 20 km and a lower crustal layer of variable thickness with 6.2 km s^{-1}, overlying an 8.2 km s^{-1} mantle half-space. Only the direct waves (first onsets) out to a distance of 100 km were used. *S* arrivals were weighted with 0.5 for three-component readings and with 0.25 for vertical component records. Based on tests with locating quarry blasts and refraction survey shots, epicentral coordinates calculated for the Läufelfingen cluster, which is recorded with excellent azimuthal coverage, are accurate within ±1 km. With four stations at very close epicentral distances, estimated uncertainty for the focal depth of this cluster is about 2 km. The Günsberg cluster is situated outside the main part of the station array, so that its location is more uncertain. Nevertheless, one of the three-component stations (BAL) with both *P* and *S* readings is close enough to place good constraints on the focal depth. Thus estimated uncertainties for both the epicentre and focal depth of this cluster are about 2 km.

EVENT TYPES AND FOCAL MECHANISMS

Based on the examination of seismograms plotted at the normal scale of 1 or 2 cm s^{-1}, the relative arrival-time differences between stations as well as the differences

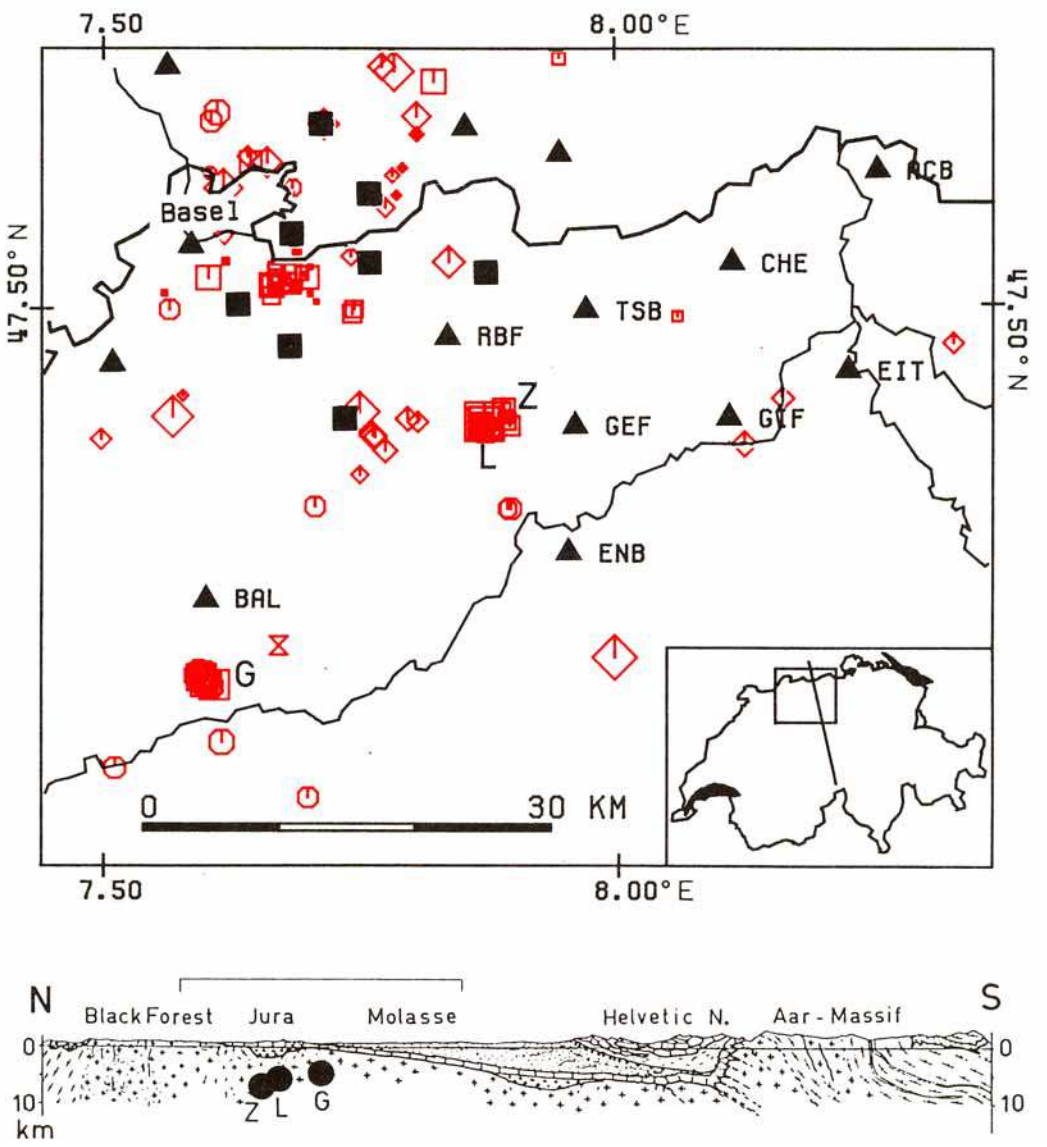

Figure 1. Epicentre map (1984–1990) of the central part of northern Switzerland (geological cross-section after Diebold & Müller 1984). The inset shows the location of the mapped region and of the geological section with respect to an outline of Switzerland. The earthquake clusters are marked by G (Günsberg), L (Läufelfingen) and Z (Zeglingen). The named triangles are the seismic stations used for the relative locations. The unnamed triangles are stations operated by the University of Karlsruhe and the squares denote the temporary eight-station array east of Basel. Different epicentre symbols correspond to different focal-depth ranges: octagon <6 km, square 6–12 km, diamond 13–24 km, hourglass >24 km.

between *S* and *P* arrivals are practically identical for all events in each cluster. Differences in hypocentre locations are thus smaller than what can be resolved by ordinary location methods. Whereas changes in the directions of first motions at some of the stations are evidence for more than one type of focal mechanisms within the same cluster, seismograms of different events with the same focal mechanism recorded at a particular station exhibit almost identical waveforms. In what follows, we want to discuss the relation between signal character and focal mechanism, based on a few selected signals. Additional signal examples can be found in a paper by Scherbaum, Gillard & Deichmann (1991) and the whole set of seismograms of both clusters recorded by the local telemetry array has been published in an earlier report (Deichmann 1990).

Table 1. Absolute locations of the three earthquake clusters.

Cluster	Date	Latitude	Longitude	Depth
Günsberg	07.-16.4.87	47.255 N	7.605 E	6
Läufelfingen	10.-17.4.87	47.428 N	7.870 E	7
Zeglingen	15.-18.4.88	47.436 N	7.889 E	9

Fig. 2 shows the seismograms, recorded at station RBF, of the 13 events from the Günsberg cluster, which were detected by both the local digital network and the national network. Despite the almost identical arrival-time differences between *S*- and *P*-waves and the obvious similarity between the individual waveforms, a closer look reveals differences in amplitude ratios of the *S* and *P* phases between the first nine and the last four events. In fact, there is a slight change in the focal mechanism that occurred between January 9 and 12, which is also evidenced by a

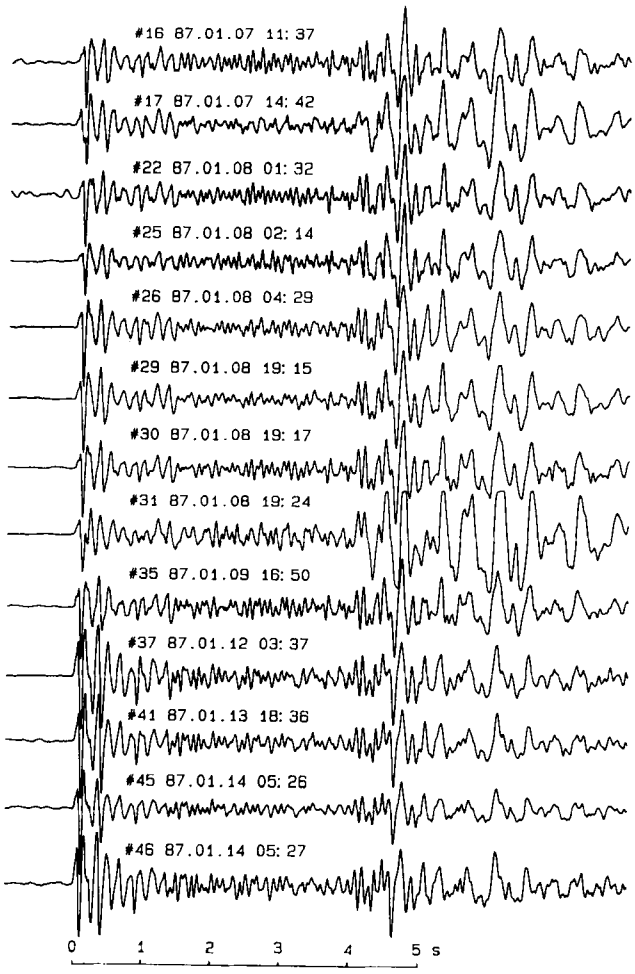

Figure 2. Seismograms at station RBF of the 13 events of the Günsberg cluster which were recorded by both the national and the local telemetry networks. Note the different P/SV amplitude ratios between the first nine events (type I) and the last four (type II).

change of first-arrival polarity at one of the stations of the local array east of Basel. This arrival plots at the periphery of the fault-plane solution with an azimuth of 204° and leads to a slight anticlockwise rotation of the NNE–SSW striking nodal plane (see Fig. 8a and Table 5). Moreover, small irregularities relative to the other seismograms are also visible in the first two cycles of the P phase as well as in the S phase of event nr. 17 and 31. In the first case, these irregularities, which are present also on all other stations and are a possible indication of non-uniform slip during this event, preclude a successful application of the cross-correlation method discussed further on.

As can be seen in Figs 3 and 4, the Läufelfingen sequence exhibits a greater diversity of signal forms. Despite the nearly identical $S-P$ times of all these events, which suggests tight clustering of the hypocentres, the changes of first motion polarity and the differences in signal character are evidence for several different focal mechanisms in this sequence. In fact, a compilation of all the available directions of first motion leads to a classification of the events into seven different types. Types I and II constitute the majority of all events; their fault-plane solutions are shown in Fig. 10. Because of the weakness of the events, the fault-plane solutions of the remaining types are not well constrained, but the available first motion polarities are sufficient to identify them as separate focal mechanisms (Deichmann 1990). However, all seven event types are predominantly strike–slip mechanisms with consistent NW–SE trending P axes.

MAGNITUDES AND TEMPORAL EVOLUTION

One of the features that distinguish an earthquake swarm from a foreshock–mainshock–aftershock sequence is the pattern of energy release with time. Since neither the national seismograph network nor the local telemetry array detected all events, we used the records of the temporary array of continuously recording seismographs to derive a complete and consistent set of magnitude values for the two clusters. In order to convert the voltage amplitudes of the uncalibrated portable recorders to magnitude values, we fitted a regression model to those events in each cluster which were also recorded by one of the stations of the local telemetry network, assuming a relation of the form:

$$M = a + b \log D_i + c_i \log A_i + d_i$$

($i = 1$, number of stations),

where M is the local magnitude calculated from the maximum amplitudes of the reference station (RBF, chosen for its proximity to the temporary network), A_i is the maximum peak-to-peak amplitude in volts, D_i is the epicentral distance in km, and a, b, c_i and d_i are the coefficients to be determined.

After determination of the coefficients, the same formula was used to calculate the magnitudes of all events, thus assuring internal consistency of the magnitude values over each earthquake series. The results are given in Tables 2 and 3. The magnitudes given by Deichmann (1990) are based on a more heterogeneous set of seismograms and thus, in some cases, differ by up to 0.3 units from the values given here.

The magnitude values were then converted to energy using the formula given by Richter (1958),

$$\log E = 2.9 + 1.9M - 0.02M^2,$$

where E is the energy in joules and M is the local magnitude.

The temporal evolution of the radiated seismic energy, expressed for each event in per cent of the total energy released over each sequence, is plotted in Figs 5 and 6. Eight out of 46 events in the Günsberg series were responsible for more than 70 per cent of the energy release. After a first period of activity, dominated by type I events and lasting almost four days, there was a quiet period, about one day long, and then activity resumed with the type II events, which lasted for another five days. During the Läufelfingen series, on the other hand, 34 of the 37 events occurred within the first 48 hours of the week long activity, and 89 per cent of the total energy was released in a single earthquake of magnitude 3.4. Thus the temporal evolution of the two sequences was quite different from one another (note the different ordinate scales in Figs 5 and 6). Whereas

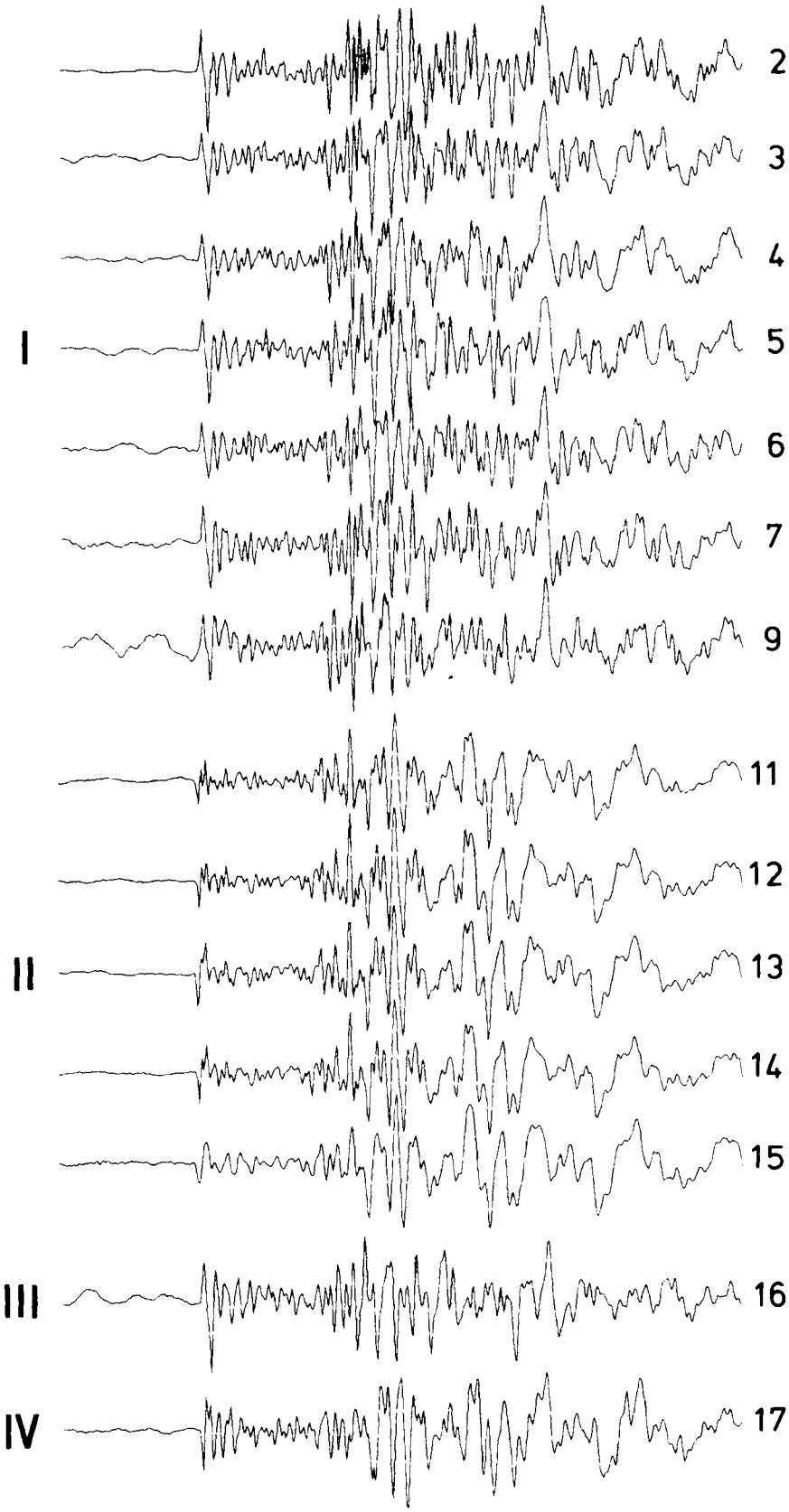

Figure 3. Vertical-component seismograms of the Läufelfingen cluster recorded at station GEF. Arabic numerals correspond to the event numbers in Table 2 and Figs 9 and 11. Roman numerals denote the different event types, which correspond to differences in focal mechanism. The three strongest events are not included here, since their signals are severely clipped at this station.

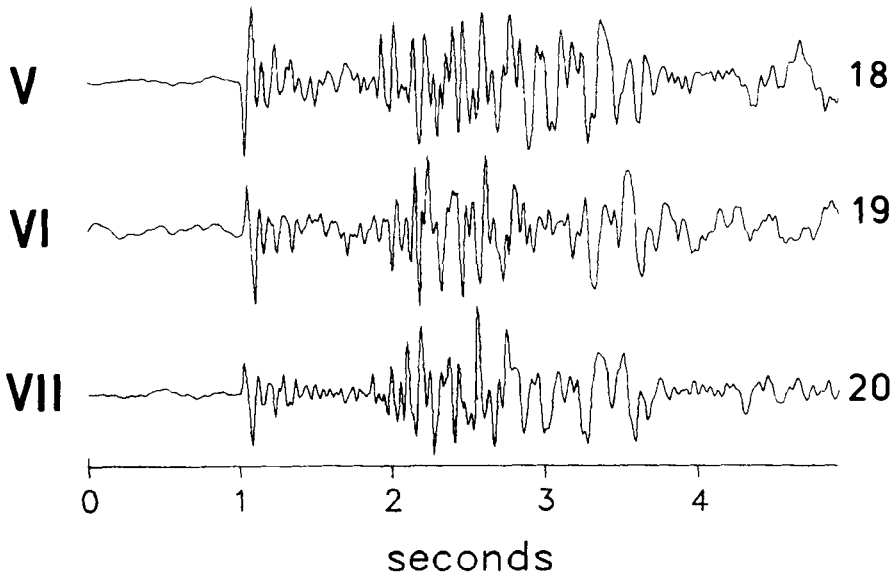

Figure 3. (*Continued*)

the Günsberg sequence has a clear swarm-like character, with a very irregular pattern of energy release, the Läufelfingen events could also be characterized as a foreshock–mainshock–aftershock sequence.

CROSS-CORRELATION AND RELATIVE LOCATION TECHNIQUE

The striking similarity between most of the signals suggests using a cross-correlation technique to resolve whatever relative arrival-time differences and consequently whatever differences in hypocentre locations might exist between individual events of a particular cluster. The ultimate goal of such a procedure is the precise relocation of all events within a given cluster relative to a chosen master event. If the cluster is sufficiently small, ray paths from the hypocentres to the stations will be essentially identical for all the events in the cluster. Therefore, systematic errors due to an incorrect velocity model will be the same for all events and will have no effect on the accuracy of the relative locations. The only source of error affecting the results are differences in the way arrival times are determined for each event. Even slight errors in picking the arrival times of the master event will affect only the absolute location of the cluster and the corresponding traveltime residuals. Provided that such errors are identical for all events, they will not influence the locations of the events relative to each other. Consequently, even *S* arrivals, which are sufficiently strong but whose true onsets are often blurred by the *P*-wave coda or by *P*-to-*S* conversions, can be used with an accuracy comparable to the *P* arrivals, as long as the arrival times are picked at exactly the same phase in all seismograms recorded at a given station. The purpose of the cross-correlation is to ensure that arrivals are determined identically for all events.

The cross-correlation method used here, which operates directly on the seismograms in the time domain, was adapted from a procedure that was applied to an analysis of the 1985 Remiremont swarm (Plantet & Cansi 1988) and is illustrated in Fig. 7.

Since sampling of each signal starts at an arbitrary instant, the maximum of the discrete cross-correlation function is not the same as the maximum of the idealized continuous signal. This is why the peak of the cross-correlation values is not symmetrical about the maximum value. In order to obtain a better approximation to the continuous cross-correlation function, a quadratic curve is fitted by a least-squares method through the discrete points that form the convex part of the maximum peak of the cross-correlation. The position of the maximum of this interpolation curve is then used to calculate the onset time of the slave event relative to the master event. In this way it is possible to resolve time differences that are smaller than the sampling interval of the data. Because the correlation function is given as a sum of the products of corresponding values, the position of the maximum will reflect the lag at which maxima and minima of the signals match best. This position will not necessarily agree completely with matching first breaks of a particular phase. However, since all the signals are processed in the same way, this fact does not influence the desired relative locations. The best results are obtained for events whose signals resemble each other most closely. Since the frequency content of the signals is determined largely by the magnitude of the event, the method works best for events that do not differ from each other by more than one magnitude value. In the presence of high- or low-frequency noise, semblance can be improved by filtering the signals with a common bandpass filter before correlation, or, in the case of *P*-wave first arrivals from events with different focal mechanisms, by changing the polarity of one of the signals.

There are several ways to estimate the uncertainty of the time differences determined by this method. Where three-component records with sufficiently high signal-to-noise ratios are available, differences between the results of separate correlations of the three components give a first indication of the possible scatter. With data sampled at an interval of 10 ms, in general this scatter amounts to 1 or 2 ms for *P*-waves and to 3 or 4 ms for *S*-waves. The increased scatter for the *S*-waves is possibly due to different amounts

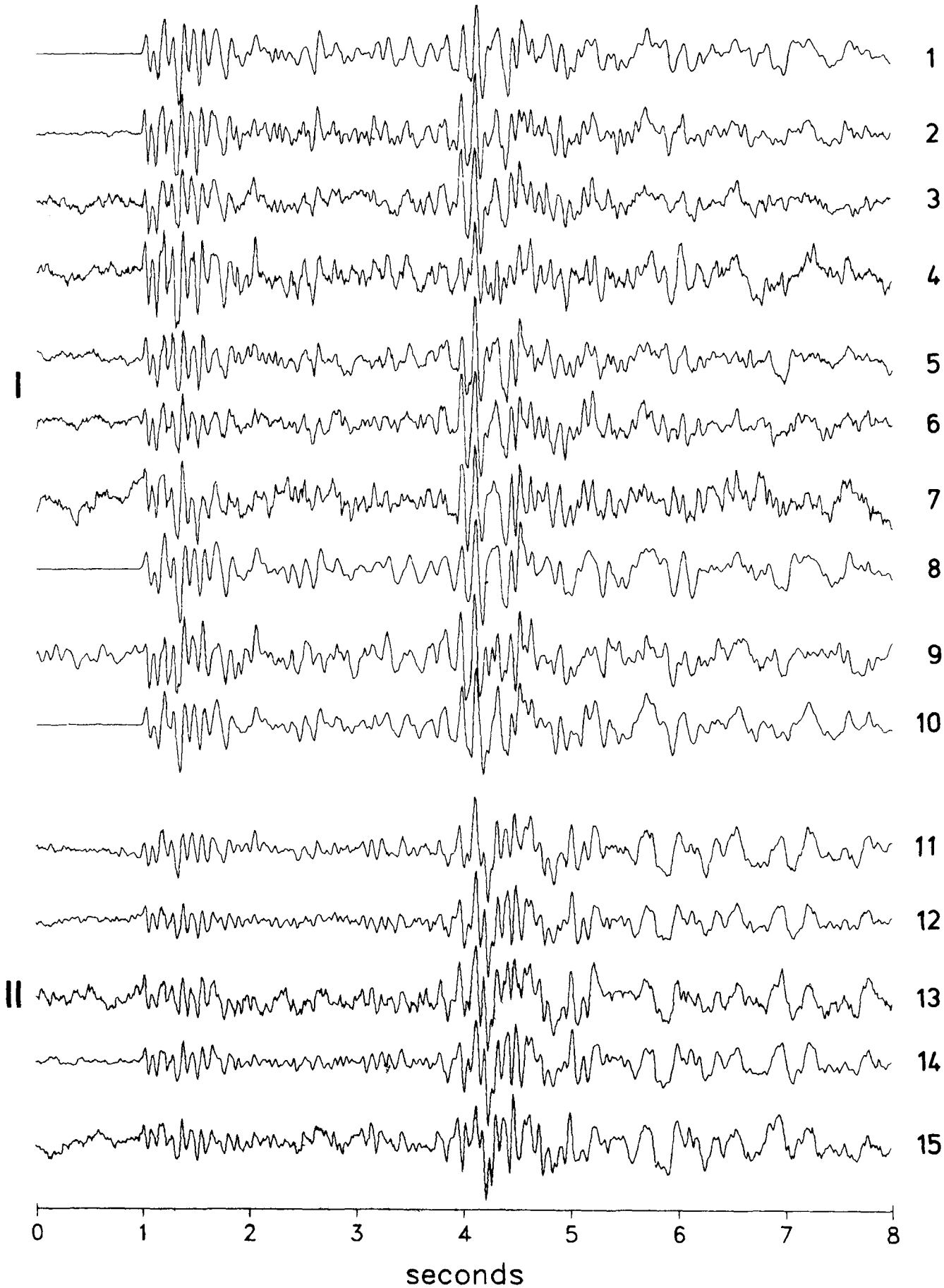

Figure 4. Horizontal-component seismograms (types I and II) of the Läufelfingen cluster recorded at station CHE. Because of the higher dynamic range of this station, the signals of the three strongest events (Nr.1, 8 and 10) are not clipped.

Table 2. List of events of the Günsberg sequence.

Date	Time	Mag	Type	Nr
87.01.07	11:37	2.2	I	16
87.01.07	11:49	1.9	I	
87.01.07	13:00	2.0	I	
87.01.07	14:42	2.5	I	17
87.01.07	16:12	1.5	I	
87.01.07	16:30	1.8	I	
87.01.08	01:32	2.0	I	22
87.01.08	02:02	2.2	I	
87.01.08	02:02	2.1	I	
87.01.08	02:14	2.3	I	25
87.01.08	04:29	2.4	I	26
87.01.08	06:59	1.0	I	
87.01.08	07:58	1.9	I	
87.01.08	08:58	1.8	I	
87.01.08	10:24	1.8	I	
87.01.08	16:29	1.7	I	
87.01.08	19:15	2.4	I	29
87.01.08	19:17	2.5	I	30
87.01.08	19:24	2.6	I	31
87.01.08	20:03	1.2	I	
87.01.08	22:41	1.3	I	
87.01.09	02:09	1.1	I	
87.01.09	03:41	1.6	I	
87.01.09	10:05	1.9	I	
87.01.09	10:24	1.0	I	
87.01.09	16:31	1.9	I	
87.01.09	16:50	2.0	I	35
87.01.09	19:58	1.7	I	
87.01.10	09:56	1.0	I	
87.01.10	12:28	1.1	I	
87.01.10	13:36	0.9	I	
87.01.10	13:46	0.9	I	
87.01.10	14:09	1.8	I	
87.01.12	03:37	2.5	II	37
87.01.12	18:43	1.7	II	
87.01.13	18:36	2.3	II	41
87.01.13	20:06	1.7	II	
87.01.13	23:26	1.6	II	
87.01.13	23:31	1.9	II	
87.01.14	00:03	1.8	II	
87.01.14	04:13	1.6	II	
87.01.14	05:26	2.2	II	45
87.01.14	05:27	2.6	II	46
87.01.14	10:16	1.8	II	
87.01.15	03:08	1.2	II	
87.01.16	04:08	1.2	II	

Table 3. List of events of the Läufelfingen sequence.

Date	Time	Mag	Type	Nr
87.04.10	07:58	2.5	I	1
87.04.10	08:23	2.1	I	2
87.04.10	10:51	1.5	I	3
87.04.10	12:44	1.6	I	4
87.04.10	18:31	1.6	I	5
87.04.10	18:33	1.5	I	6
87.04.10	22:24	1.3	I	7
87.04.11	02:44	1.1	I	
87.04.11	03:14	3.4	I	8
87.04.11	03:15	1.9	I	9
87.04.11	03:21	1.4	I	
87.04.11	03:24	1.0	II	
87.04.11	03:24	1.3	I	
87.04.11	03:24	1.0	II	
87.04.11	03:25	1.0	II	
87.04.11	03:45	1.0	I	
87.04.11	04:10	1.5	I	
87.04.11	05:23	1.3	I	
87.04.11	05:50	1.3	II	
87.04.11	06:04	1.5	III	
87.04.11	07:21	2.8	I	10
87.04.11	09:06	1.5	II	11
87.04.11	09:59	1.3	III	16
87.04.11	13:14	1.1	I	
87.04.11	13:16	1.1	II	
87.04.11	13:16	1.8	II	12
87.04.11	13:16	1.2	II	
87.04.11	13:17	1.3	II	13
87.04.11	14:22	1.6	II	14
87.04.11	14:50	1.5	IV	17
87.04.12	05:18	1.0	II	
87.04.12	05:23	1.3	II	
87.04.12	05:25	1.5	II	15
87.04.12	05:26	1.1	II	
87.04.14	17:06	1.3	V	18
87.04.15	13:25	1.2	VI	19
87.04.17	17:41	1.1	VII	20

of *P*-wave energy present in the *S*-wave train on each of the three components. Another indication of the reproducibility of the results is obtained by repeating the correlations with all possible combinations of master and slave events within a given set of events. This test is equivalent to closing a polygon in triangulation measurements. The discrepancy between the results obtained from different master events is a direct measure for the confidence of the individual determinations. In addition, by applying a least-squares adjustment procedure, it is possible to determine arrival-time differences between master and slave events which minimize these discrepancies. The mathematical formulation of such a procedure is given in the Appendix. With data sampled at intervals of 10 ms and good quality arrivals, the discrepancies for *P*-waves was rarely greater than 2 ms, with an average that was often less than 1 ms. For *S*-waves it was somewhat higher, caused in part by greater variations in signal form.

The Läufelfingen cluster was relocated using only the local telemetry array recorded at station CHE, where all channels are digitized with the same clock. Because the Günsberg cluster lies outside this station array, sufficient depth resolution was only attainable by also using the data

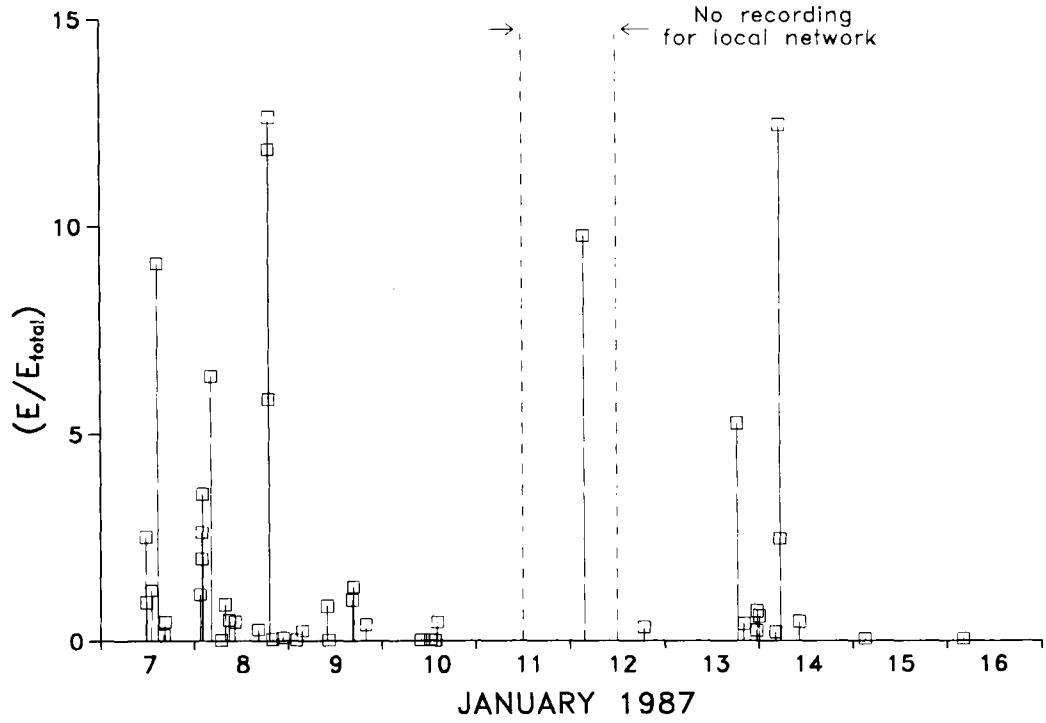

Figure 5. Energy release (in per cent of the total energy) versus time for the Günsberg sequence.

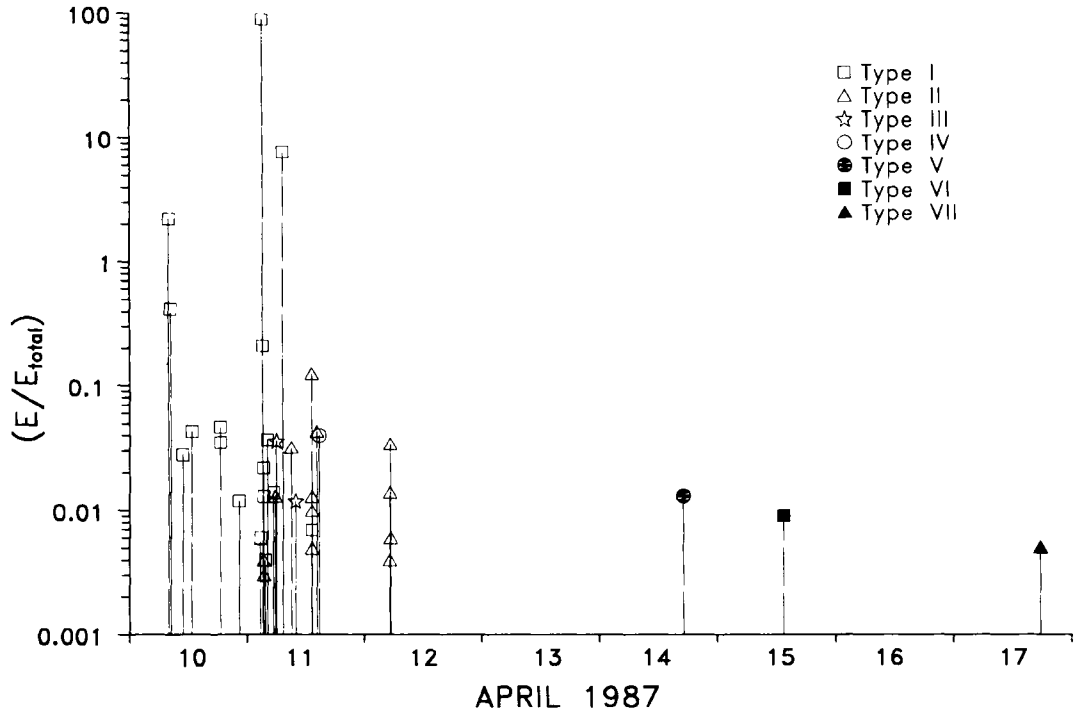

Figure 6. Energy release (in per cent of the total energy) versus time for the Läufelfingen sequence.

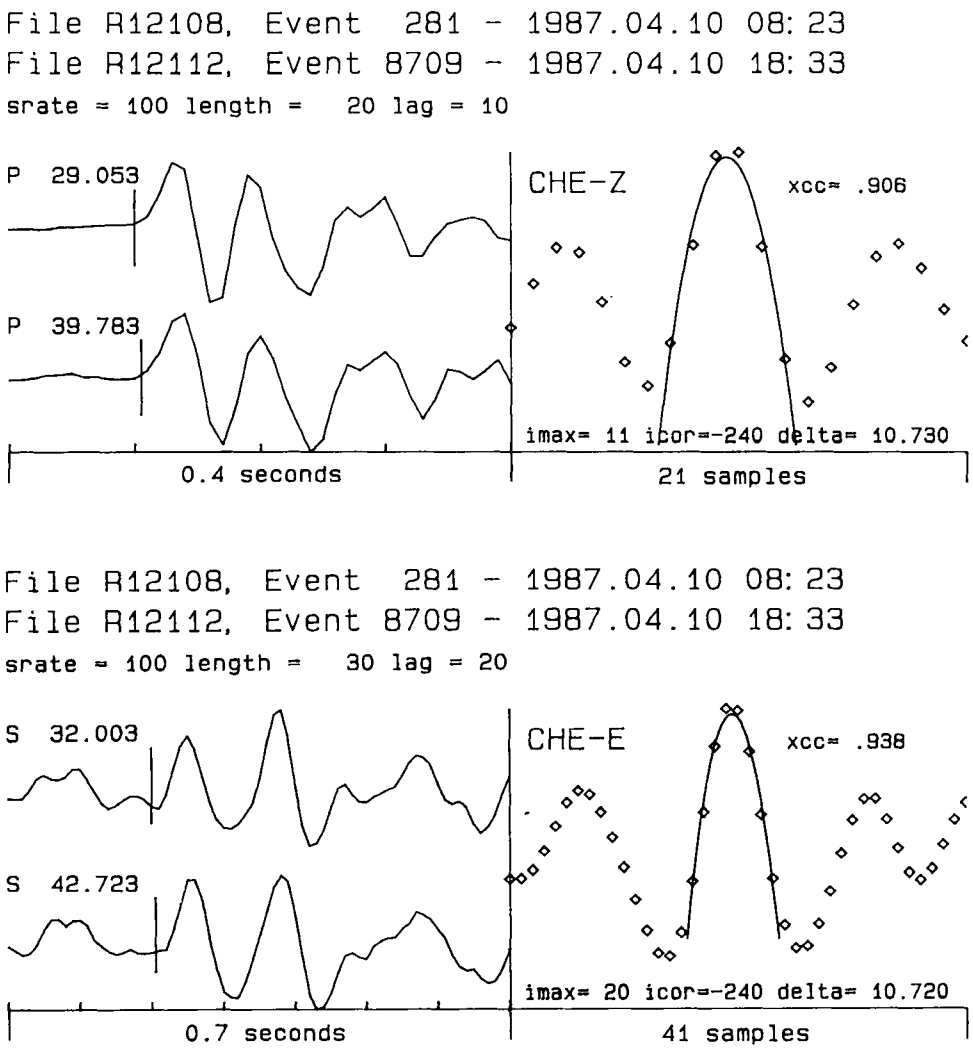

Figure 7. Cross-correlation example for the *P*-waves on the vertical component of station CHE (top) and of the *S*-waves on the E–W component (bottom). The top trace of each signal pair is the master event. The tick marks correspond to 0.1 s. Sampling rate is 100 Hz. For the *P*-wave correlation a time window 0.2 s long was shifted between maximum lags of ±0.1 s. For the *S*-waves the time window was 0.3 s and the maximum lag 0.2 s. The vertical bar on the traces of the master event shows the arrival time picked by eye, while on the lower trace it shows the corresponding arrival determined from the correlation. The small diamonds in the right side of each diagram denote the discrete values of the cross-correlation for each shift of one sampling interval. The continuous curve is the parabola fitted by least squares through the peak of the discrete values. The resulting time differences between the arrivals of master and slave (in seconds relative to the dates and times in the headline) are given by the value *delta*. The correlation coefficient is denoted by *xcc*.

of station BAL. This station is part of an other array with a different clock, consequently its $S-P$ times had to be used in the location procedure (see the discussion in the Appendix). Only the seismic velocities in the immediate neighbourhood of the epicentres influence the relative locations, so a model with a constant *P*-wave velocity of 5.9 km s^{-1} and a ratio between *P* and *S* velocities of 1.71 was used. The algorithm used for performing the master-event location is essentially a single-event hypocentre location program, in which the arrival times of the slave events, as determined from the correlation procedure, are corrected with the traveltime residuals of the master event. These residuals are thus treated as station corrections. The corrected arrivals were then weighted with the reciprocal of their estimated uncertainties. These weights take into account the different quality of the cross-correlations at each station, but were chosen to be the same for both the master and the slave events. A standard iterative least-squares algorithm, which inverts the normal equations by Gauss–Jordan elimination, was used to solve for the hypocentral coordinates and the origin time (e.g. Menke 1989). As a consequence of the way the arrival times were weighted, the standard deviations of the solutions are given directly by the square root of the diagonal elements of the inverse matrix of the normal equations. With uniform azimuthal station coverage, the error bars calculated in this way give realistic estimates of the uncertainty of the results. As demonstrated by Monte Carlo simulations, under unfavourable circumstances, the major axes of the error ellipsoid may be rotated with respect to the chosen coordinate axes, so that the calculated standard deviations will underestimate the actual uncertainty of the locations. For this reason, conservative estimates for the uncertainties of the arrival times derived from the cross-correlations were used in the location

algorithm. For the Günsberg cluster the calculated standard deviations of the relative epicentral coordinates and the depth are 20–30 m and 40–60 m respectively, while for the Läufelfingen cluster the corresponding values are 10–20 m and 20–30 m. The relocation of the three refraction survey shots demonstrated that, if the sources are close enough to each other to exclude lateral velocity variations, the method outlined above gives reliable results (Deichmann 1987).

RESULTS

Günsberg

The results of the relative location of the Günsberg cluster, based on the cross-correlation method described above and on the least-squares adjustment procedure explained in the Appendix, are displayed in an epicentre plot and in two vertical cross-sections in Fig. 8. Event Nr.30 was chosen as the common master event. As mentioned earlier, variations in signal character and a change of first-motion polarity at one of the stations close to the NNE–SSW striking nodal plane are evidence for two slightly different focal mechanisms in the Günsberg series; the corresponding fault-plane solutions are also plotted in Fig. 8. The strike of the two nodal planes of the first focal mechanism type are well constrained by the first-motion data alone. The horizontal directions of the two vertical cross-sections were chosen to correspond to the strike of these two nodal planes. In the vertical cross-section in Fig. 8(b), most of the hypocentres appear to lie on a WNW–ESE striking plane which dips to the NNE with 63° (denoted by the oblique line in Fig. 8b). Only the position of two events (Nr.25 and 31)

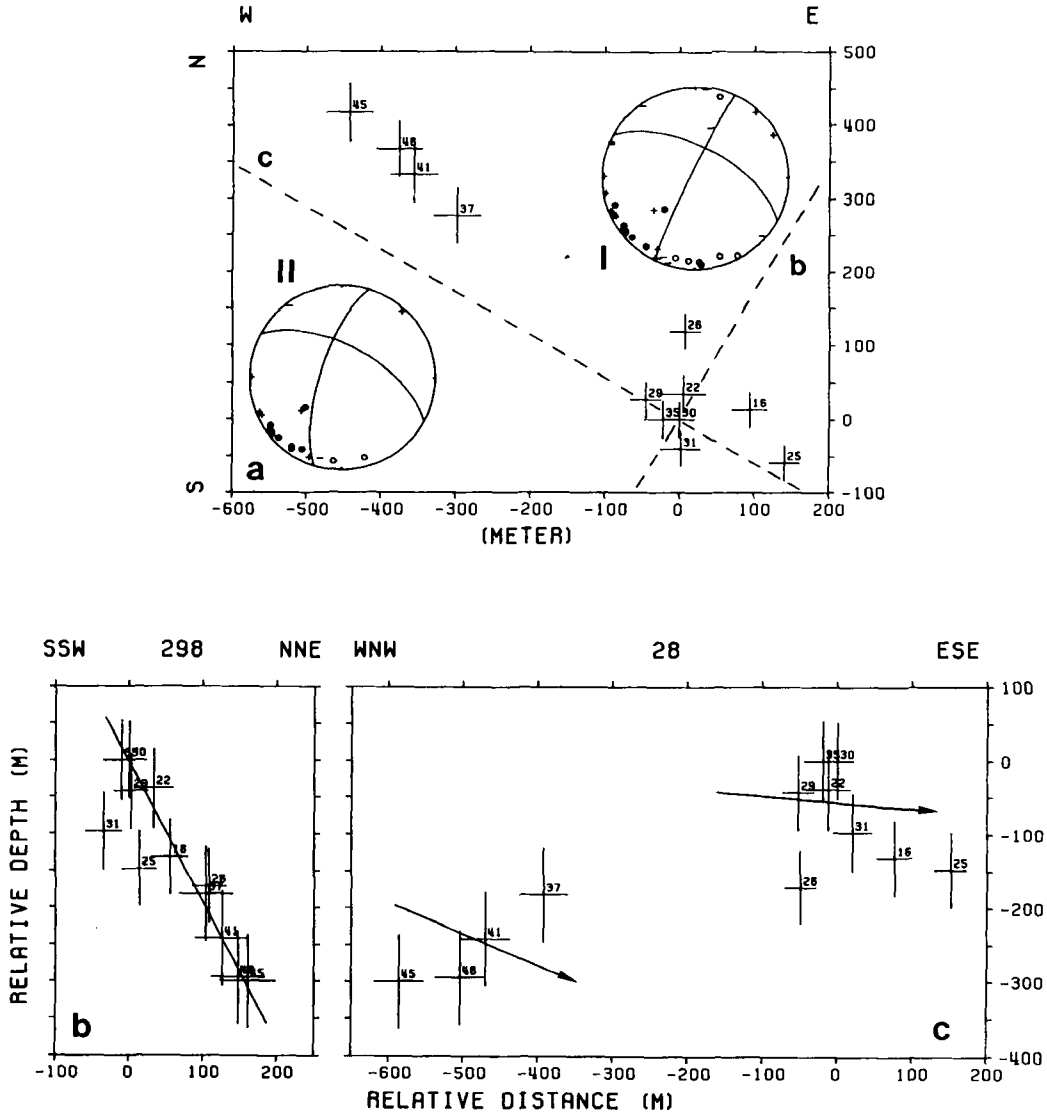

Figure 8. Relative locations of the Günsberg cluster: epicentres (a) and projections of the hypocentres onto two mutually perpendicular vertical planes (dashed lines, b and c). The size of the crosses is proportional to the calculated standard deviations of the respective coordinates. The depth cross-section (b) is perpendicular to the active fault plane, indicated by the oblique line. In the projection parallel to the active fault plane (c), the arrows indicate the direction of slip of the hanging-wall relative to the foot-wall for the events of type I (upper right) and of type II (lower left), corresponding to the two fault-plane solutions (equal area, lower hemisphere) in (a). Full circles and plus signs indicate impulsive and emergent compression; empty circles and minus signs indicate impulsive and emergent dilatation. For absolute locations see Table 1.

deviates by more than one standard deviation from this plane. In the case of event Nr.31, the residuals of the least-squares adjustment were signficantly larger than for the other events, which is probably due to the somewhat different signal character mentioned earlier and to the generally lower frequency content of this event. The four type II events are separated from the other events not only in time, but as Fig. 8(a) and (c) show, also in space. It is thus possible to view the two event types as two separate clusters. On the other hand, it is likely that the hypocentres of some of the remaining smaller events, which could not be relocated, actually fill this apparent gap.

The dip of the nodal planes is not well constrained by the first-motion data alone. However, strike and dip of fault planes which are compatible with both the first-motion data and the spatial distribution of hypocentres are limited to a very small range (±10°). Moreover, the NNE–SSW striking nodal plane cannot correspond to the active fault plane common to both the type I and II events. Otherwise, the hypocentres plotted in Fig. 8(c) would have to be aligned along a line that is vertical or dipping from left to right, which is clearly not the case. If one views the type I and II events as belonging to two separate clusters, then one could also find two separate planes with different inclinations that fit both the hypocentral distribution and the available first-motion data. However, the only minor differences in signal character and in first-motion polarities preclude any really significant differences in focal mechanism. Therefore, based on all the available evidence, both event types must be associated with the same fault, and the difference in focal mechanism is reflected in the slightly different orientation of the slip vectors (Fig. 8c). On the other hand, to visualize a real fault as a perfect plane is probably a gross oversimplification. Thus, the focal mechanism change can also result from a slight bend or offset of the fault, which however is not resolvable with the attainable location accuracy.

Nevertheless, there is no doubt from these results that the earthquake swarm of Günsberg was associated with right-lateral motion, with a slight normal faulting component, along a WNW–ESE striking fault. The active part of this fault extends over at least 750 m horizontally and 300 m vertically.

Läufelfingen

For the Läufelfingen series the correlation and relative location procedure was applied to 10 events of type I and five events of type II. Because of the diversity in signal character between event types and because several records of the three strongest events were severely clipped, the cross-correlation could not be performed for all events relative to the same master event. Instead, the data set was first subdivided into three subsets (type I with $M \geq 2.1$, type I with $M \leq 2.1$ and type II), and the master event location was performed separately for each subset. In a second step, two of these master events were relocated relative to the third (Nr.2 in Table 3 and Figs 9 and 11).

In the resulting epicentral plot (Fig. 9a), the locations of type I and II events cannot be separated from each other, and together they cluster along a N–S direction. A projection of the hypocentres onto a vertical N–S striking

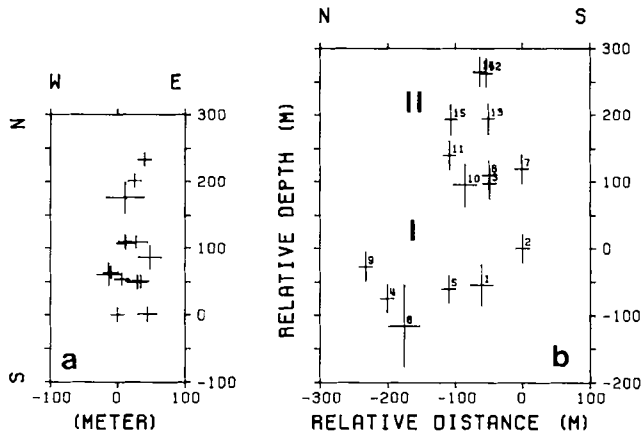

Figure 9. Relative locations of the Läufelfingen cluster: epicentres (a) and projection of the hypocentres onto a vertical plane striking N–S (b). The size of the crosses is proportional to the calculated standard deviation of the respective coordinates. For absolute locations see Table 1.

plane reveals their planar distribution and also shows that the two event types occupy separate depth ranges (Fig. 9b). Because of the fact that the events of type I and II had to be relocated relative to two separate master events, the location of the events of type II as a whole and of the three events with $M > 2.1$ relative to the weaker type I events is subject to an added uncertainty of the same order of magnitude as the error bars (one standard deviation) of the individual events. Moreover, the results shown here for the Läufelfingen cluster are based on a single cross-correlation, without performing the least-squares adjustment between all possible event pairs explained in the Appendix. In order to check the results, a subsequent correlation of all possible event pairs was performed only for the type I events with $M \leq 2.1$. The differences between the results given here and the relative locations for this event subset, based on the adjusted arrival-time differences, lie within the calculated standard deviations.

Although slightly different, the fault-plane solutions of both the type I and II events correspond to strike-slip focal mechanisms with roughly N–S and E–W striking nodal planes. From what was said in the preceding paragraph it is clear that the hypocentres lie on a more or less vertical plane striking N–S rather than E–W. In fact, a projection of the type I hypocentres onto a vertical plane perpendicular to the nodal plane striking 10° E of N shows that they align almost perfectly along a line with a slope that corresponds to the westward dip of that nodal plane (Fig. 10b). A similar good agreement is obtained for the type II events, when plotted in a vertical projection perpendicular to the nodal plane that strikes 8° W of N (Fig. 10a). These results are unequivocal evidence that at least all the type I and II events of the Läufelfingen series (31 out of a total of 37 events) are a result of sinistral strike-slip motion on two steeply dipping and more or less N–S oriented faults. The geometrical relationship between the individual hypocentres and the fault orientations is shown more clearly in Fig. 11. The rectangular perimeter of the fault planes in Fig. 11 is entirely arbitrary and was chosen only for the sake of enhancing the three-dimensional effect of the diagram. Moreover, the planar representation of the fault is certainly

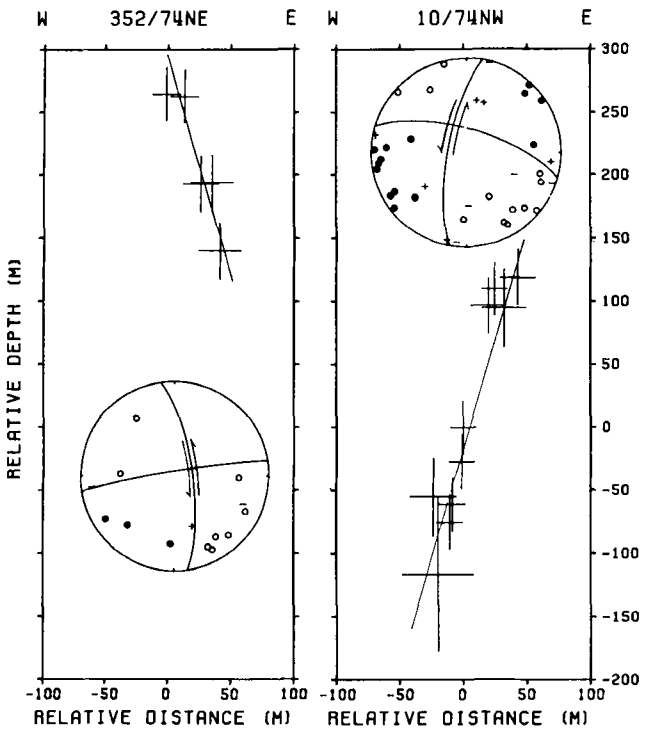

Figure 10. Projections of the hypocentres onto vertical planes perpendicular to the two more or less N–S striking nodal planes for the type II events (left) and the type I events (right). The oblique lines correspond to the projections of the active fault planes, indicated by double arrows in the respective fault-plane solutions (equal area, lower hemisphere; see also caption to Fig. 8).

a grossly simplified picture of a surface that in nature is much more irregular. Thus it is possible that what has been treated here as two separate fault planes, corresponding to the two main focal mechanisms, are actually two differently oriented parts of a single irregularly shaped fault with various bumps and bends.

THE ZEGLINGEN TRIPLET

Between 1988 April 15 and 18, almost exactly a year after the Läufelfingen swarm, four more small earthquakes with magnitudes between 1.1 and 1.9 occurred near the town of Zeglingen (Table 4). Their hypocentres, based on HYPO71 locations, were situated 2 km to the NW and 2 km deeper than the cluster of Läufelfingen. In spite of the tight clustering of these four hypocentres, as indicated by the very small traveltime differences, only the first three events are characterized by identical waveforms (Deichmann 1990). The third event was sufficiently strong to yield a reasonably well-constrained fault-plane solution. The resulting focal mechanism for this triplet of similar events corresponds to an almost pure normal fault with a NE–SW oriented T-axis (Fig. 12a). Application of the cross-correlation and relative location procedure shows that the maximum separation between these three hypocentres is only 50–60 m (Fig. 12b, c, d). Projections of the hypocentres onto vertical planes perpendicular to the two nodal planes clearly demonstrate that rupture must have occurred on the fault plane striking NW–SE and dipping steeply to the NE (Fig. 12c).

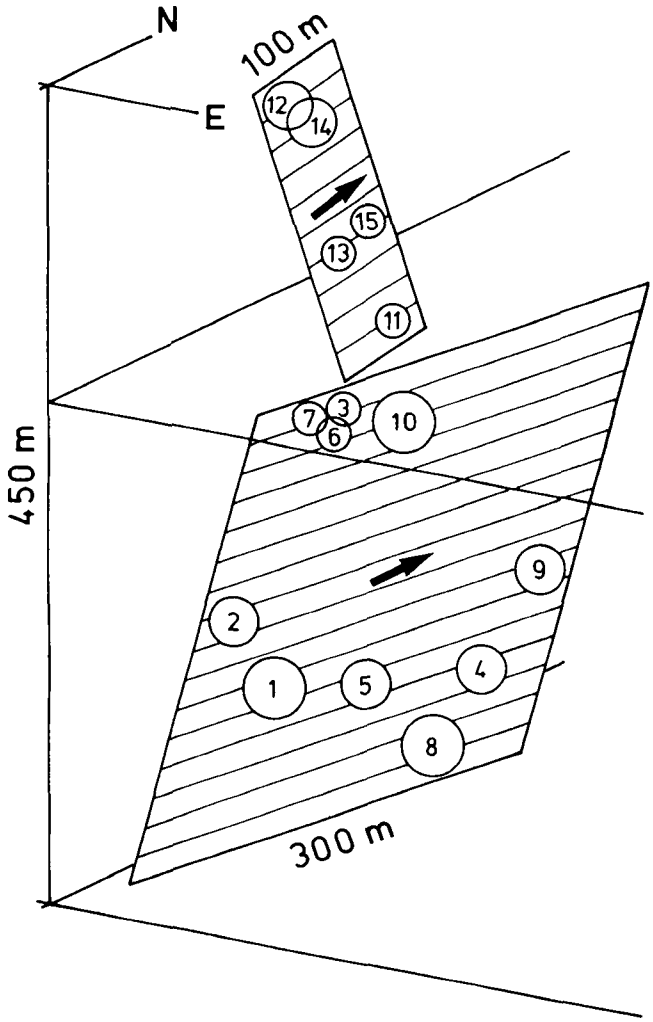

Figure 11. Fault-planes of the Läufelfingen cluster. The number of each event corresponds to the number in Table 2 and indicates the temporal sequence of occurrence. The size of the circles is a qualitative indication of the magnitude of each event (small: $1.3 \leq M \leq 1.5$; medium: $1.6 \leq M \leq 2.1$; large: $2.5 \leq M \leq 3.4$). Arrows indicate the direction of slip on the fault of the foot-wall for type I events (bottom) and of the hanging-wall for type II events (top).

DISCUSSION AND CONCLUSIONS

As shown by the examples discussed in this paper, a procedure to determine precise relative arrival times based on a cross-correlation of the seismograms from a cluster of similar earthquakes is a powerful tool to map the spatial distribution of the hypocentres within the cluster and to resolve the details of the rupture geometry. The least-squares adjustment of the traveltime differences

Table 4. List of events of the Zeglingen sequence.

Date	Time	Mag	Type	Nr
88.04.15	14:12	1.5	I	8806
88.04.15	21:29	1.1	I	8807
88.04.16	14:05	1.9	I	199
88.04.18	14:06	1.5	II	8808

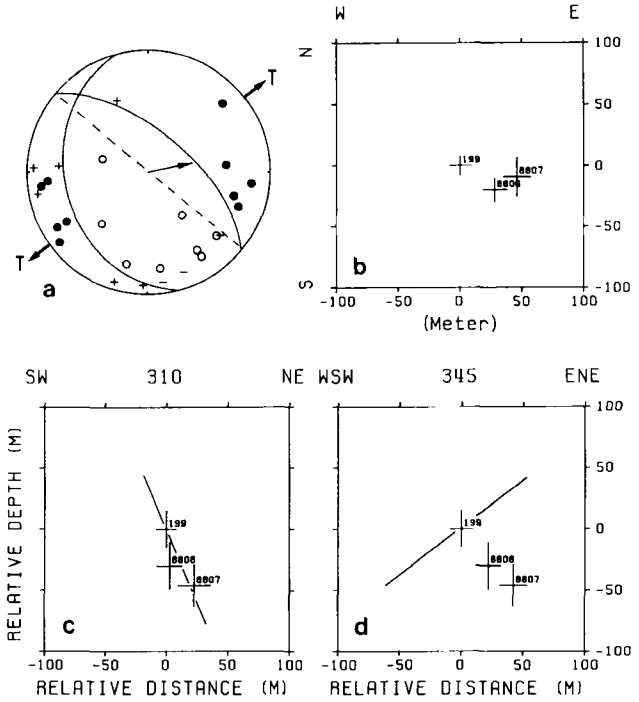

Figure 12. Fault-plane solution (equal area, lower hemisphere) for the Zeglingen triplet (a) and relative locations: epicentre plot (b) and projections of the hypocentres onto vertical planes perpendicular to the two nodal planes (c and d). The oblique lines in (c) and (d) are the traces of the two nodal planes in the respective projections. For absolute locations see Table 1.

presented in the Appendix is an added refinement, which increases and provides quantitive estimates of the precision of the method.

Based on the analysis of the two earthquake clusters of Läufelfingen and Günsberg it has been possible to demonstrate for the first time that both N–S striking faults with left-lateral slip and WNW–ESE striking faults with right-lateral slip are active below the Jura Mountains of northern Switzerland. Whereas the former are also visible in the surface geology, the latter are not (Fig. 13). The orientation of these two sets of strike–slip faults as well as of the normal fault activated by the Zeglingen triplet is consistent with the general NNW–SSE direction of maximum horizontal compression and the corresponding WSW–ENE directed extension (Fig. 13 and Table 5), which is characteristic of northern Switzerland (Pavoni 1980, 1987; Deichmann 1990).

In addition to contributing to a more detailed picture of the regional deformation, the results presented here demonstrate unequivocally that clusters of similar earthquakes correspond to a swarm-like activity, caused by repeated slip on the same fault. If both tectonic stress and frictional strength were constant over the whole fault, the stress release would occur in a single event. The spatial and temporal characteristics observed in such swarm-like earthquake clusters is clearly an expression of a heterogeneous fault structure and of complex patterns of stress release.

It is important to note that there is no regular relationship between the time of occurrence of the individual earthquakes and their position on the fault. Instead of a sequential migration in a preferred direction across the fault, we see how the events seem to occur at different places on the fault in a highly erratic manner. Even the separation in time between the type I and II events in the Läufelfingen series, indicated in Fig. 11, is only apparent. As can be seen from Table 3, there was a time period of almost 10 hours during which both event types occurred together. Moreover, the time interval between successive events of the same type can vary between less than a minute and several hours. This erratic space–time distribution of the individual earthquakes seems to be a characteristic feature of such swarm events. The same irregular behaviour can be seen in the Günsberg series, even though the occurrence of the two different event types is clearly separated in time (Fig. 8), and was also noted in the six-event cluster near Winterthur, where the time interval between successive events varied from a few hours to two years (Deichmann 1987). During the 1984–85 Remiremont sequence, Plantet & Cansi (1988) noted the same type of erratic behaviour that is observed here, together with a progressive migration of hypocentres towards the periphery of the fault. In an analysis of microearthquake clusters in Japan, Nishigami (1987) showed that the rupture areas of individual events belonging to the same fault overlap. For the Läufelfingen cluster an order of magnitude estimate of the source radius (200–300 m) of the strongest event ($M = 3.4$) shows that the area which ruptured during this event includes the locations of most if not all of the other type I events (the lower fault plane in Fig. 11).

Given that the frictional strength resisting slip is anything but uniform over the surface of a fault, there are basically two ways to envisage the mechanism that causes sequences of similar earthquakes.

In the first scenario, the individual events are triggered by temporal fluctuations of the driving shear stress, which are the consequence of local stress concentrations following each event. The time delay between events is then a function of the rate of stress redistribution as well as of stress corrosion on the periphery and on the patches left unbroken by the previous rupture. This would imply that even relatively small earthquakes ($M < 4$) can have very complex sources, in which slip propagates around previously ruptured patches and unbroken barriers (e.g. Nishigami 1987). Since in each event rupture is restricted to those areas which were left unbroken by previous events and which are not strong enough to act as barriers, this mechanism does not require that overlapping source areas correspond to zones of repeated slip. However, assuming that the weakening of the fault due to stress corrosion is not a primary factor, and given that the weakest patches will be the first to slip, this mechanism requires that the stress concentrations in the unbroken patches increase from one event to the next. Such a local increase in shear stress would have to occur despite the fact that the average shear stress acting on the fault would be expected to decrease as a consequence of the stress released by each event.

In the second scenario, the individual events would be triggered by short-term variations of the local frictional resistance on the fault. These variations could be caused most simply by changes in the effective stress due to fluctuations of pore fluid pressure. Given that in certain parts of the earth's crust fluids exist at suprahydrostatic

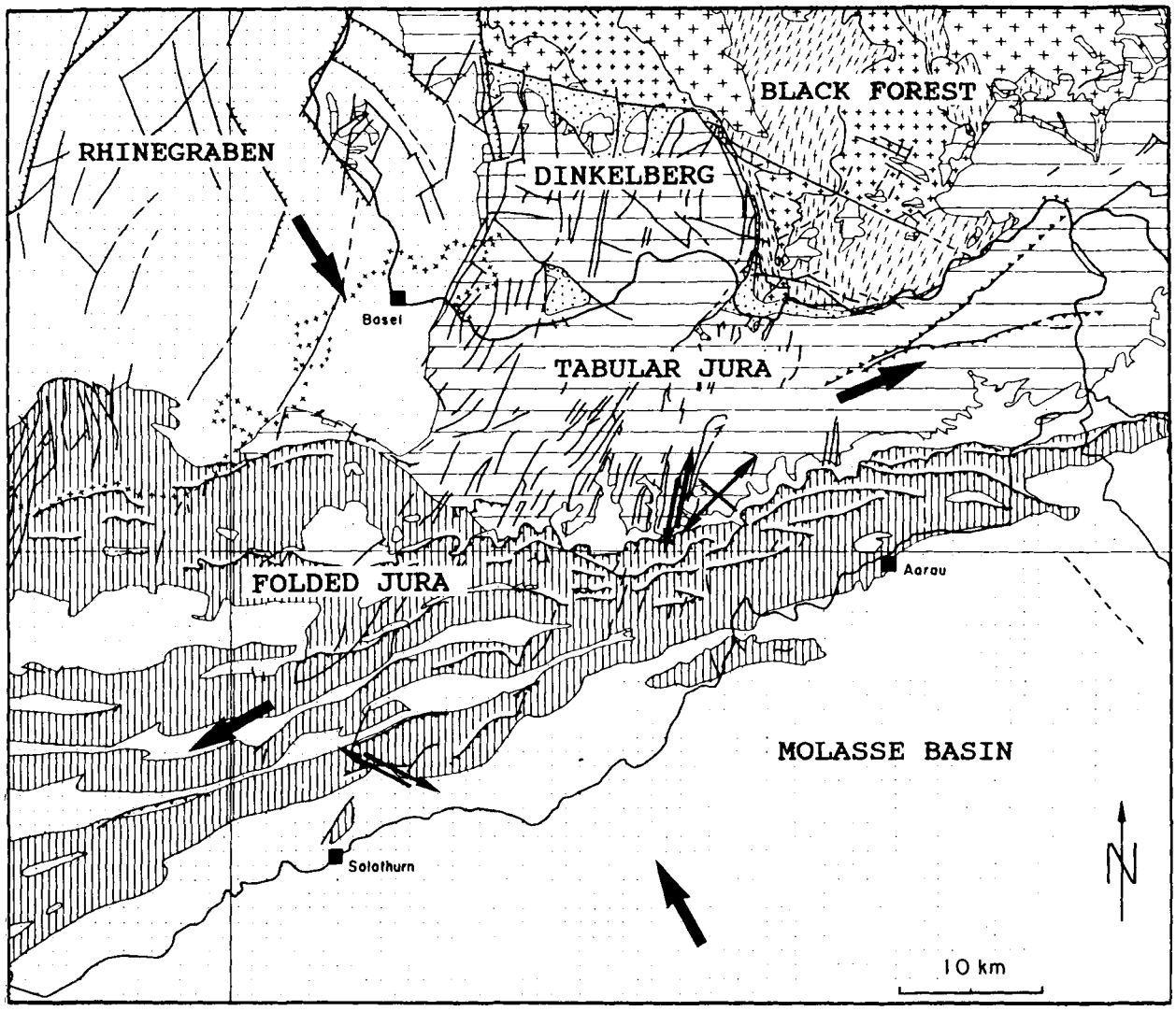

Figure 13. Tectonic map (from Diebold & Müller 1984) with orientations of faults and directions of slip. The large arrows show the directions of maximum crustal shortening and extension.

pressures (Fyfe, Price & Thompson 1978) and that some degree of shear stress of tectonic origin is ubiquitous, it is easy to see how such fluids, as they migrate upwards through pre-existing zones of weakness, can trigger repeated slip on the same fault. Depending on the pressure and amount of available fluids as well as on the detailed geometry and surface structure of a particular fault, both the spatial and temporal pattern of the resulting seismic activity will exhibit great variability (Sibson 1981; 1990). Since shear stress on a patch that has broken during a particular event will have fallen only to the level of the frictional strength in effect at the time of that event, a further weakening of the fault due to an increase of fluid pressure can easily lead to repeated slip on overlapping source areas.

Table 5. Focal mechanism parameters. Nodal planes: strike and dip with direction of dip. *P* and *T* axes: azimuth and plunge. For hypocentral parameters see Table 1.

Event	Faultplane	Aux.plane	P-axis	T-axis
Günsberg type I	298/62NE	205/85NW	158/23	255/16
Günsberg type II	298/62NE	197/70NW	156/35	249/06
Läufelfingen type I	190/76NW	282/79NE	146/18	56/02
Läufelfingen type II	352/74NE	260/86NW	307/08	215/14
Zeglingen type I	310/63NE	165/32SW	187/67	53/16

These two models represent two end members of a wide range of possible behaviour. Even if the mechanism envisaged in the second scenario were predominant, stress concentrations at the perifery of a ruptured patch and strength heterogeneities that might manifest themselves as barriers in a particular event will have a strong influence on the actual pattern of stress release in a given earthquake sequence. It is hoped that a detailed analysis of the source parameters of each event, such as moment, source radius and stress drop, in relation to the distance and time interval between events, will help to decide which of the mechanisms suggested in these two scenarios is predominant in triggering swarm-like sequences of similar earthquakes.

ACKNOWLEDGMENTS

We thank K.-P. Bonjer and his colleagues at the University of Karlsruhe for providing numerous seismograms of their

stations in southern Germany, which were very useful in constraining the fault-plane solutions. M. Baer contributed significantly to this work with development and maintenance of the software for the data analysis of the Swiss Seismological Service's network. M. Dietiker's and M. Grieder's help with the installation and maintenance of the various instruments is also gratefully acknowledged. Critical reviews by J. Ansorge, H. Maurer, S. Faber and an additional anonymous reviewer improved the final version of the paper. This study is part of a research programme financed by Nagra, the National Cooperative for Nuclear Waste Disposal. Contribution number 709, Institute of Geophysics, ETH-Zürich.

REFERENCES

Console, R. & Di Giovambattista, R., 1987. Local earthquake relative location by digital records, *Phys. Earth planet. Inter.*, **47**, 43–49.

Deichmann, N., 1987. Seismizität der Nordschweiz, 1983–19186, *Technischer Bericht, NTB 87–05*, NAGRA, Baden.

Deichmann, N., 1990. Seismizität der Nordschweiz, 1987–1989, und Auswertung der Erdbebenserien von Günsberg, Läufelfingen und Zeglingen, *Technischer Bericht, NTB 90–46*, NAGRA, Baden.

Diebold, P. & Müller, W. H., 1984. Szenarien der geologischen Langzeitsicherheit: Risikoanalyse für ein Endlager für hochaktive Abfälle in der Nordschweiz, *Technischer Bericht, NTB 84–26*, NAGRA, Baden.

Fréchet, J., 1985. Sismogenese et doublets sismiques, *PhD thesis*, University of Grenoble.

Fremont, M.-J. & Malone, S. D., 1987. High precision relative locations of earthquakes at Mount St. Helens, Washington, *J. geophys. Res.*, **92**, 10 223–10 236.

Fyfe, W. S., Price, N. J. & Thompson, A. B., 1978. *Fluids in the Earth's Crust*, Elsevier, Amsterdam.

Geller, R. J. & Mueller, C. S., 1980. Four similar earthquakes in Central California, *Geophys. Res. Lett.*, **7**, 821–824.

Hamaguchi, H. & Hasegawa, A., 1975. Recurrent occurrence of the earthquakes with similar wave forms and its related problems, *Zisin (J. Seism. Soc. Japan), Ser. 2*, **28**, 153–169 (in Japanese with English abstract).

Ito, A., 1985. High resolution relative hypocenters of similar earthquakes by cross-spectral analysis method, *J. Phys. Earth*, **33**, 279–294.

Ito, A., 1990. Earthquake swarm activity revealed from high-resolution relative hypocenters—clustering of microearthquakes, *Tectonophysics*, **175**, 47–66.

Lee, W. H. K. & Lahr, J. C., 1972. *HYPO-71, a computer program for determining hypocenter, magnitude and first motion pattern of local earthquakes*, US. Geol. Survey Open File Report.

Logan, A. L. L., 1987. Accurate Relative Location of Similar Earthquakes, *PhD thesis*, University of Edinburgh.

Menke, W., 1989. *Geophysical Data Analysis: Discrete Inverse Theory*, International Geophysics Series, vol. 45, Academic Press, San Diego, CA.

Nakamura, Y., 1978. A_1 moonquakes: Source distribution and mechanism, *Proc. Lunar planet. Sci. Conf. 9th*, 3589–3607.

Nishigami, K., 1987. Clustering structure and fracture process of microearthquake sequences, *J. Phys. Earth*, **35**, 425–448.

Pavoni, N., 1980. Crustal stresses inferred from fault-plaine solutions of earthquakes and neotectonic deformation in Switzerland, *Rock Mech.*, Suppl. 9, 63–68.

Pavoni, N., 1987. Zur Seismotektonik der Nordschweiz, *E. Geol. Helv.*, **80**, 461–472.

Pechmann, J. C. & Thorbjarnardottir, B. S., 1990. Waveform analysis of two preshock–mainshock–aftershock sequences in Utah, *Bull. seism. Soc. Am.*, **80**, 519–550.

Plantet, J. L. & Cansi, Y., 1988. Accurate epicenters location with a large network, example of the 1984/1985 Remiremont sequence, in *Seismic Hazard in Mediterranean Regions*, pp. 347–358, eds Bonnin, J., Cara, M., Cisternas, A. & Fantechi, R., Kluwer Academic Publ.

Poupinet, G., Ellsworth, W. L. & Fréchet, J., 1984. Monitoring velocity variations in the crust using earthquake doublets: an application to the Calaveras Fault, California, *J. geophys. Res.*, **89**, 5719–5731.

Richter, C. F., 1958. *Elementary Seismology*, Freeman, San Francisco. CA.

Scherbaum, F., Gillard, D. & Deichmann, N., 1991. Slowness power spectrum analysis of the coda composition of two microearthquake clusters in northern Switzerland, *Phys. Earth. planet. Inter.*, **67**, 137–161.

Scherbaum, F. & Wendler, J., 1986. Cross spectral analysis of Swabian Jura (SW Germany) three-component microearthquake recordings, *J. Geophys.*, **60**, 157–166.

Sibson, R. H., 1981. Fluid flow accompanying faulting: field evidence and models, in *Earthquake Prediction: an International Review*, pp. 593–603, Maurice Ewing Series Vol. 4, eds Simpson, D. W. & Richards, P. G., Am. Geophys. Union.

Sibson, R. H., 1990. Rupture nucleation on unfavourably oriented faults, *Bull. seism. Soc. Am.*, **80**, 1580–1604.

Slunga, R., Norman, P. & Glans, A. C., 1984. *Seismicity of southern Sweden*, FOA Report C 20543-T1, Nat. Defence Res. Inst., Stockholm.

Tsujiura, M., 1983a. Waveform and spectral features of earthquake swarms and foreshocks—in special reference to earthquake prediction, *Bull. Earthq. Res. Inst. Tokyo, Univ.* **58**, 65–133.

Tsujiura, M., 1983b. Characteristic frequencies for earthquake families and their tectonic implications: evidence from earthquake swarms in the Kanto District Japan, *Pure appl. Geophys.*, **4**, 573–600.

VanDecar, J. C. & Crosson, R. S., 1990. Determination of teleseismic relative phase arrival times using multi-channel cross-correlation and least-squares, *Bull. seism. Soc. Am.*, **80**, 150–169.

APPENDIX: LEAST-SQUARES ADJUSTMENT OF RELATIVE ARRIVAL TIMES

From the lag at which the cross-correlation of the ith and jth event recorded at a particular station has its maximum we obtain a value for the arrival-time difference between the ith and jth event.

$$\Delta_{ij} = (t_i + c_i) - (t_j - c_j) + e_{ij} = t_{ij} + c_{ij} + e_{ij}$$

$$(i = 2, \ldots, n; j = 1, \ldots, n-1; i > j), \qquad \text{(A1)}$$

Δ_{ij} is the arrival-time difference between the ith and jth event, measured by cross-correlation; $t_{ij} = t_i - t_j$ is the true arrival-time difference; $c_{ij} = c_i - c_j$ is the clock error: difference of synchronization of recording instrument between the ith and jth event; and e_{ij} is the error of the cross-correlation of the ith with the jth event.

From (A1) it can be seen that there are two distinct sources of errors. The e_{ij} is inherent in the cross-correlation procedure and is caused by the combination of finite sampling rate, limited frequency bandwidth of the signal and imperfect signal similarity, which is due to small differences in source and path as well as to additive noise. The c_{ij}, on the other hand, is introduced by the recording instrument

when it assigns a time to the first sample of each seismogram, and is caused by drifts of the internal clock in between events or by jitter in decoding radio-broadcasted time signals.

Given n events recorded at a particular station, there are a maximum of $n(n-1)/2$ combinations of events satisfying (A1). For locating a group of events relative to a master event (to which we arbitrarily assign the index $j=1$) we need to determine the $n-1$ arrival-time differences, t_{i1} ($i=2,\ldots,n$). For $i \geq 3$ and $j \geq 2$ with $i > j$, we can express Δ_{ij} as a difference between Δ_{i1} and Δ_{j1}; designating the difference calculated in this way by Δ'_{ij} and using (A1), we get:

$$\Delta'_{ij} = \Delta_{i1} - \Delta_{j1} = (t_i - t_j) + (c_i - c_j) + (e_{i1} + e_{j1})$$
$$= t_{ij} + c_{ij} + (e_{i1} - e_{j1}). \quad \text{(A2)}$$

Since in general $e_{i1} - e_{j1} \neq e_{ij}$, it follows that $\Delta'_{ij} \neq \Delta_{ij}$.

Provided we have more than two events and have performed the cross-correlation for all possible event pairs, we obtain a system of $n(n-1)/2$ linear equations for $n-1$ unknowns, which can be solved by the method of least squares. The system of equations has the following form:

$$(t_{i1} + c_{i1}) - \Delta_{i1} = r_k \quad (i = 2,\ldots,n; k = 1,\ldots,n-1),$$
$$(t_{i1} + c_{i1}) - (t_{j1} - c_{j1}) - \Delta_{ij} = r_k$$
$$(i = 3,\ldots,n; j = 2,\ldots,n-1; k = n,\ldots,n(n-1)/2). \quad \text{(A3)}$$

Here t_{i1}, t_{j1}, c_{i1} and c_{j1} are not the true arrival-time differences and clock discrepancies but only the estimates of these quantities, subject to the condition that the sum of the square of the residuals

$$\sum_{k=1}^{n(n-1)/2} r_k^2 \quad \text{(A4)}$$

be minimal. VanDecar & Crosson (1990) used a similar procedure to determine accurate arrival-time differences for a single teleseismic event recorded at different stations of a seismograph network. In their algorithm, the first $n-1$ equations in (A3) are replaced by a zero mean constraint, which makes their problem non-singular.

The fact that there is no way to determine t_{i1} and c_{i1} separately has some important consequences. If all stations employed in the relative location procedure are recorded by the same instrument with a single clock controlling the A/D-converter, then different timing errors between events, relative to some absolute time, are the same for all stations. In this case, only the calculated origin times of the events will be affected and thus the clock error can be ignored. If, on the other hand, signals are recorded at each station by individual recorders, each with its own clock or time-signal receiver, the clock error must be taken into account. If the error is less than or comparable to the error of the cross-correlation, it must be treated as an additional uncertainty to be considered in one's estimate of the relative arrival-time errors. Alternatively, since the clock errors at each station are equal for both the P and S phase in a given signal, the effects of clock errors can also be eliminated by using only $S-P$ arrival-time differences in the relative location algorithm.

Therefore, bearing in mind that clock errors may be of significance, we replace the expressions in brackets on the left-hand side of equations (A3) by τ_{i1} and τ_{j1}, respectively. Then in matrix notation we can write (A3) as

$$\mathbf{A}\boldsymbol{\tau} - \boldsymbol{\Delta} = \mathbf{r}. \quad \text{(A5)}$$

As an example we write out the case for $n = 4$:

$$\begin{pmatrix} 1 & 0 & 0 \\ 0 & 1 & 0 \\ 0 & 0 & 1 \\ -1 & +1 & 0 \\ -1 & 0 & +1 \\ 0 & -1 & +1 \end{pmatrix} \begin{pmatrix} \tau_{21} \\ \tau_{31} \\ \tau_{41} \end{pmatrix} - \begin{pmatrix} \Delta_{21} \\ \Delta_{31} \\ \Delta_{41} \\ \Delta_{32} \\ \Delta_{42} \\ \Delta_{43} \end{pmatrix} = \begin{pmatrix} r_1 \\ r_2 \\ r_3 \\ r_4 \\ r_5 \\ r_6 \end{pmatrix}. \quad \text{(A6)}$$

One way to solve this problem, subject to the least-squares condition (A4), leads to the well-known set of normal equations (e.g. Menke 1989),

$$\mathbf{A}^T\mathbf{A}\boldsymbol{\tau} - \mathbf{A}^T\boldsymbol{\Delta} = 0, \quad \text{(A7)}$$

which can be inverted to yield the desired solution,

$$\boldsymbol{\tau} = (\mathbf{A}^T\mathbf{A})^{-1}\mathbf{A}^T\boldsymbol{\Delta}. \quad \text{(A8)}$$

The simple nature of matrix $\mathbf{A}$ would in principle allow us to give an analytical expression for $\boldsymbol{\tau}$ as a linear combination of the elements of $\boldsymbol{\Delta}$. However, due to insufficient waveform similarity, in particular when magnitude differences are large, the cross-correlation often cannot be performed with satisfactory results for all possible combinations of event pairs, so that the elements of $(\mathbf{A}^T\mathbf{A})^{-1}$ are not only a function of the number of events but also of the number of computed correlations. In addition, one might want to give different weights to individual correlations, using for example the correlation coefficient as a measure of their quality. Thus in practice, it is more expedient to solve for $\boldsymbol{\tau}$ numerically. To avoid computational errors due to manipulating small differences of large numbers, it is advisable to reduce the elements of $\boldsymbol{\Delta}$ to a small value by subtracting days, hours and minutes from them, before setting up the normal equations.